Title
Elucidation of the Active Site for the Oxygen Evolution Reaction on a Single Pt Atom Supported on Indium Tin Oxide

Journal
The Journal of Physical Chemistry Letters, 14(10)

ISSN
1948-7185

Authors
Kumari, Simran
Sautet, Philippe

Publication Date
2023-03-16

DOI
10.1021/acs.jpclett.3c00160

Elucidation of Active Site for the Oxygen Evolution Reaction on Single Pt Atom Supported on Indium Tin Oxide

Simran Kumari[†] and Philippe Sautet[*, †, ‡]

†Chemical and Biomolecular Engineering Department, University of California, Los Angeles, CA 90095, USA

‡Chemistry and Biochemistry Department, University of California, Los Angeles, CA 90095, USA

*E-mail: sautet@ucla.edu

ABSTRACT

Single-atom catalysts (SACs) have attracted attention for their high catalytic activity and selectivity, but the nature of their active sites under realistic reaction conditions, involving various ligands, is not well understood. In this study, we use Density Functional Theory calculations and grand canonical basin hopping to theoretically investigate the active site for the oxygen evolution reaction (OER) on single Pt atom supported on Indium Tin Oxide, including the influence of the electrochemical potential. We show that the ligands on the Pt atom change from Pt-OH in the absence of electrochemical potential to $PtO(OH)_4$ in electrochemical conditions. This change of the chemical state of Pt is associated to a decrease of 0.3V for the OER overpotential. This highlights the importance of accurately identifying the nature of the active site under reaction conditions and the impact of adsorbates on the electrocatalytic activity. This theoretical investigation enhances our understanding of SACs for OER.

TOC Graphic

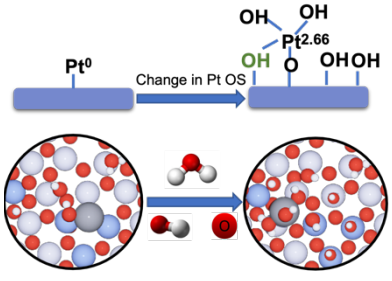

Modification of the Pt Active site in oxygen evolution conditions

Keywords: Single-atom catalysts, Oxygen Evolution Reaction, Supported Catalysts, Active Site under reaction condition, Density Functional Theory.

Single-atom catalysts (SACs), with their potential maximized atom utilization efficiency, have attracted significant attention due to their high catalytic activity and selectivity[1,2]. These catalysts have been applied to a large range of reactions, including CO oxidation,[3–8] hydrogenation[9], dehydrogenation[9,10] and other electrocatalytic reactions[11–13]. For the expensive and in-demand noble metal catalysts like Ir, Pd, and Pt, SACs represent an ultimate dispersion of the metal with all the atoms exposed[14–16] and, if activity remains high compared to nanoparticle catalysts, an optimal utilization and cost. Additionally, SACs might open up particular reaction pathways, different from that of larger particles, and are well suited for a molecular-level understanding of the active-site structure and reaction mechanism by utilizing a variety of element-specific analytical tools supplemented by in situ/operando characterization and coupled with computational modeling[5,17–19]. There are now strong evidence that SACs are not static catalysts, but that they respond to reaction conditions by adapting their set of ligands and their mode of interaction with the support, making the determination of the active site challenging[20] Significant effort has been devoted to obtaining a thorough understanding of SACs through unique characterization techniques and theoretical calculations[21–23].

The oxygen evolution reaction (OER) is a key bottleneck in the electrocatalytic water splitting process, which is a promising method for producing hydrogen in an environmentally friendly manner[24–31] . The two half-processes that makeup water splitting, hydrogen, and oxygen evolution reactions (HER and OER) are carried out in acidic or alkaline environments, but the high overpotential required for OER in acidic conditions has limited the efficiency of acidic water electrolysis, despite its other advantages such as higher current density and pressure[32]. While numerous materials have been studied for OER, a lack of efficiency, durability, and high cost have hindered their widespread industrial use. Single-atom catalysts (SACs) have received significant attention for their potential to improve the efficiency and durability of OER catalysts, as they have a large fraction of exposed active sites, high durability, and good stability in aggressive environments[33].

In the oxygen evolution reaction (OER), oxygen gas is produced from water through a 4-electron transfer process. This means that four electrons are transferred from the anode to the cathode during the reaction, which drives the production of oxygen gas. The OER elementary mechanisms can be written as:

$$H_2O(l) + {}^* \rightarrow {}^*OH + H^+ + e^- \quad (1)$$

$$^*OH \rightarrow {}^*O + H^+ + e^- \quad (2)$$

$$H_2O(l) + {}^*O \rightarrow {}^*OOH + H^+ + e^- \quad (3)$$

$$^*OOH \rightarrow {}^* + O_2(g) + H^+ + e^- \quad (4)$$

Where * represents the active site of the catalyst, (g) and (l) refer to the gas and liquid phase respectively, and *OH, *O, and *OOH represent the reaction intermediates adsorbed on the active site. The catalytic activity for OER is typically characterized by calculating the Gibbs free energies of the individual reaction steps as a function of the electrochemical potential defined using the standard hydrogen electrode (SHE) as a reference. The acidic mechanism involves the production of $H^+ + e^-$ pairs, and their Gibbs free energy is calculated from the equilibrium $H^+ + e^- \leftrightarrow$ ½H_2 in the SHE at standard conditions (pH = 0, pressure p_{H_2}= 1 bar, and T = 298.15 K) and using the Gibbs free energy of hydrogen gas. The reaction Gibbs free energies, which stem from the binding strength between the catalyst and OER intermediates, are affected by the electronic properties of the active site. The typical procedure widely used in the literature to calculate the reaction Gibbs free energies, ΔG_n corresponding to equations (1)–(4) at standard conditions is shown in equations in the SI-S2; more details about the derivation can be found in reference[34]

In_2O_3 is a wide bandgap semiconductor that has been used in gas sensors[35] and has also been explored as a potential catalyst for CO_2 hydrogenation[36,37] . When doped with Sn, it becomes indium tin oxide (ITO), a transparent conducting oxide with metal-like conductivity and optical transparency in the visible range. This material is used in transparent electrodes for electro-optical displays, such as liquid crystal displays and solar cells[38]. Sn-doped indium oxide has high conductivity, making it useful for electrocatalysis applications in water. Researchers have therefore been interested in using these conductive oxides as supports for Pt-metal clusters in electrocatalytic applications[39–42] .The electrochemical behavior of ITO in acidic solutions with pH 1 can be affected by dissolution at high anodic and cathodic potential. However, in our study we have taken precautions to prevent this be carefully selecting the potential window for our calculations and limiting the potential to below 2V vs SHE. This potential range has been reported in literature to result in stable ITO behaviors in acidic solutions with pH 1[43]. Following the experimental studies, we modeled the (111) surface of 5% doped ITO as our substrate model and determined that all Sn atoms prefer to reside in the surface layer, which has been previously

reported to give the maximum carrier density.[44] We chose the 111 termination for the ITO surface because it has the lowest surface energy and hence higher stability when compared to other surface terminations[45] .Eight Sn (5% atom) atoms are present in a four-layer slab with unit cell dimensions

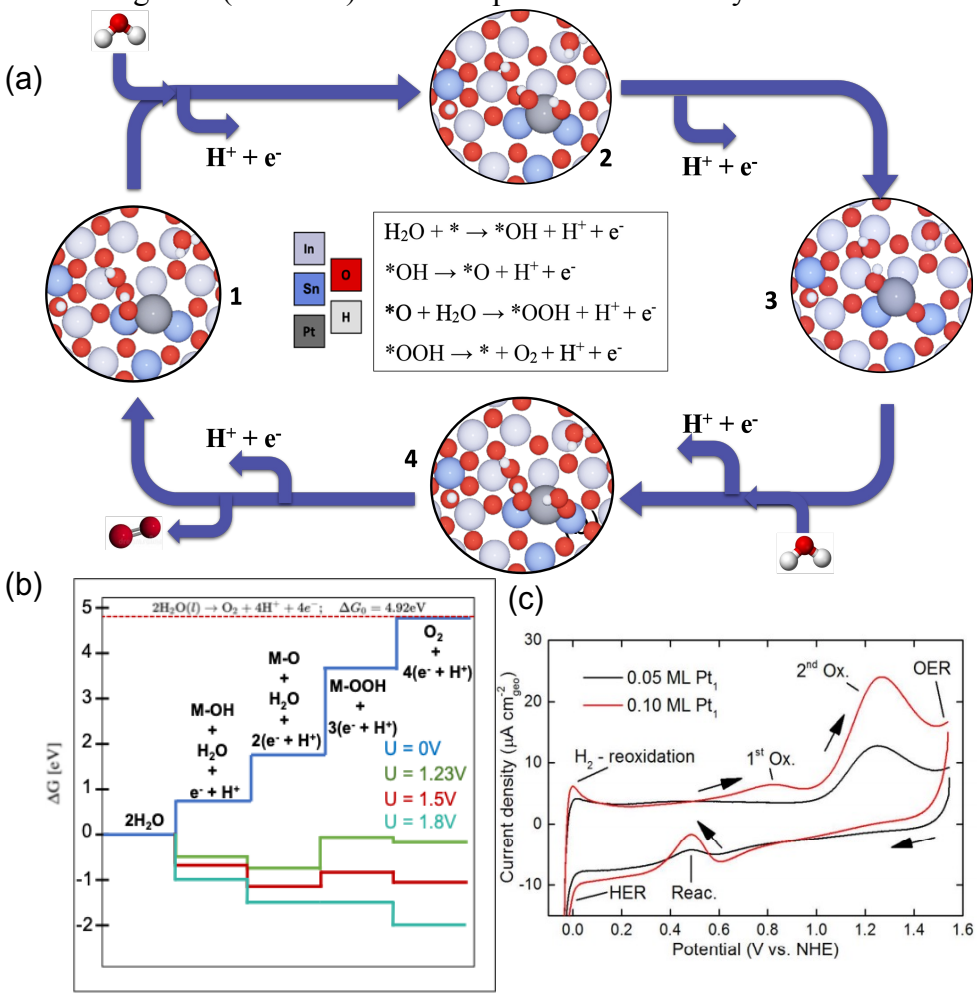

Figure 1: OER reaction mechanism on our initial structure for a Pt single atom on ITO determined in vacuum and in the absence of electrochemical potential (a) 4 electron step reaction mechanism (Blue: Sn , Light grey: In, Grey : Pt, Red : O and White : H) (b) reaction energy profile for the 4 OER reaction steps at potential U = 0 V vs SHE (Blue), U= 1.23V vs SHE (Green), U = 1.5 V vs SHE(Red) and U = 1.8 V vs SHE (Cyan). (c) experimental cyclic-voltammograms for Pt_1/ITO at 0.05 ML and 0.01 ML coverages, and for ITO, acquired at 0.1 V/sec. scan rate, reproduced from von Weber, A.; Baxter, E. T.; Proch, S.; Kane, M. D.; Rosenfelder, M.; White, H. S.; Anderson, S. L. Size-Dependent Electronic Structure Controls Activity for Ethanol Electro-Oxidation at Pt n /Indium Tin Oxide (n = 1 to 14), *Physical Chemistry Chemical Physics* 2015, *17* (27), 17601–17610. Copyright 2015 Royal Society of Chemistry.

of 14.65 x 14.65, four in the top layer and four in the bottom layer. 3 Sn atoms replace the In atoms in 5-coordinated sites, and 1 Sn atom replaces the In in the 6-coordinated sites. The unit dimension in the surface plane for the sued ITO(111) supercell is 14.65 x 14.65 Å. In electrocatalytic conditions, the ITO surface would interact with water molecules, which were found to be

dissociated on the surface (up to 2 water molecules are dissociated, and the rest are physisorbed). According to our earlier research, the presence of hydroxyls and water on the ITO surface plays a significant role in anchoring Pt single atoms (Pt-SA). The hydroxyls that are formed on the surface of ITO in the presence of water would interact with the Pt-SA and assist stabilize it by preventing it from sintering into larger clusters. We refer the reader to our earlier study for complete details on the surface and Pt-SA structure and water interaction with the surface[45] .

As a first step in investigating the OER activity on a Pt-SA/ITO system, we utilized a Pt-SA/ITO structure previously determined in our previous work [44]. The structure, shown in Fig. 1(a) as 1, consists of Pt atoms bound to two Sn atoms and one hydroxyl group in a Pt-Sn bridging position, acting as an anchor for the SA. Further details of the structure can be found in the Supporting Information (SI-S5) and in our previous work[45]. To determine the most stable adsorption site for the Pt surface complex, we employed a basin hopping method to optimize the position of the Pt atom and the movement of hydroxyls and water already present on the surface, under vacuum conditions and without considering electrochemical conditions such as pH and potential. OER was experimentally investigated on dispersed Pt atoms on ITO by Weber et al.[42] From the experimental findings reprinted in Fig 1(c), three distinct peaks in the positive sweep of the cyclic-voltammogram are seen at pH 1. On the positive-going sweep, the first and second oxidation peaks are present at 0.82 V, and 1.28 V vs SHE. Additionally, the onset for OER is seen at ~ 1.5 V. Our study focused specifically on the anodic sweep and the characterization of the oxygen evolution reaction (OER) on ITO. As a result, we did not include any computational calculations or analysis in the cathodic region. While the reactions occurring during the cathodic sweep are not the primary focus of our work, they have been thoroughly addressed in the experimental paper.With this information, we investigated the overpotential of OER on Pt-SA/ITO. The four-step OER reaction mechanism is given in Fig 1 (a), and the corresponding reaction free-energy diagram is given in Fig 1(b) for four potential values (U = 0, 1.23,1.5 and 1.9 V vs SHE) at a pH=1. The full computational details and methods are provided in the SI. For the catalytic cycle starting with our initial Pt-SA/ITO structure, we determine the third step as the rate-determining step with an overpotential of 0.57 V. This is 0.3 V higher than what is found experimentally (overpotential = 0.27 V). We interpret this high discrepancy in the overpotential values as an indication that the active center of the catalyst we are using to simulate the OER reaction mechanism, determined in

the absence of electrode polarization, is not correct. The functional groups generated in reaction conditions (positive potential vs SHE) can largely affect/modify the active site and hence should be properly investigated.

Due to the presence of water molecules, hydroxyl, and oxygen adsorbates in the OER reaction condition, it is of utmost importance to determine the true nature of the active site of the catalyst. This is very important in the case of SACs, as the metal atom is not surrounded by any other metal atoms, and the active site is more exposed to the reactants. To better understand the active site of the catalyst and the nature of the interaction with the reactants, the interaction of the Pt-SA with the hydroxyl and oxygen species needs to be explicitly studied. The characterization of SAC catalysts under realistic reaction conditions is a relatively unexplored field. However, in-situ techniques such as operando X-ray absorption spectroscopy (XAS) have demonstrated potential in understanding the dynamic electronic and local environments of these structures and identifying

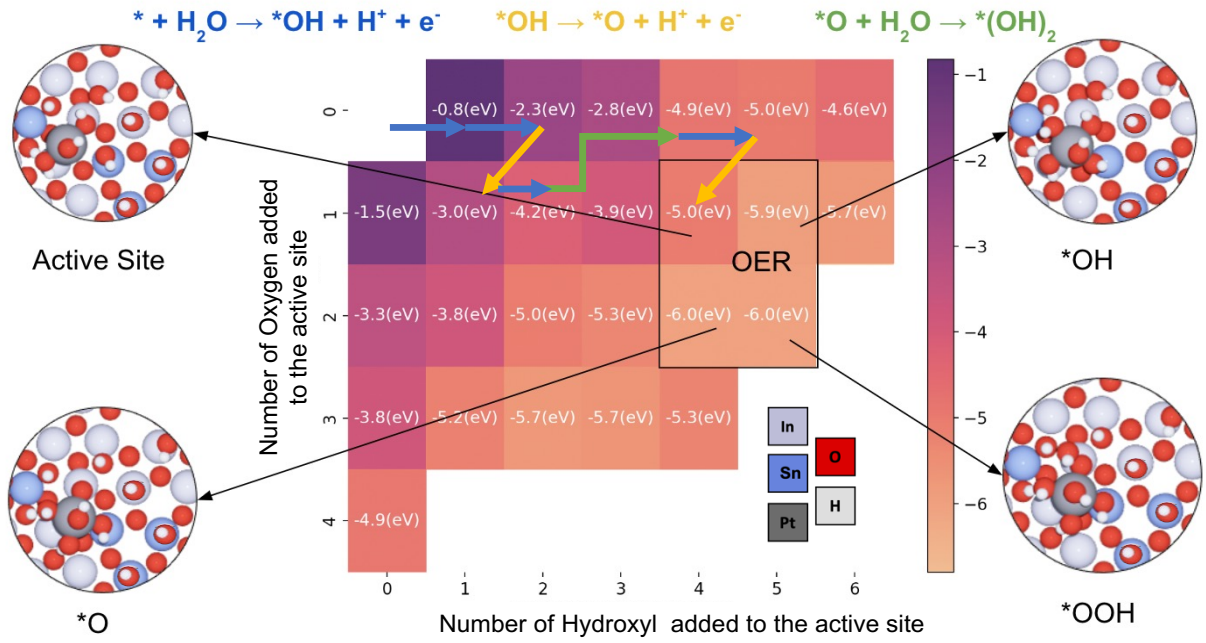

Figure 2: Free energy surface exploration via GCBH. The heat plot shows the formation energy of the active site configurations, as a function of the number of hydroxyl groups and O atoms added. The blue arrows represent the electrochemical reaction * + H_2O → OH + H^+ + e^-, the yellow arrow the electrochemical reaction *OH → *O + H^+ + e^- and the green arrow the chemical dissociative adsorption of H_2O. The black box shows the active site and intermediates of the OER mechanism. The structures of the active site along with the OER intermediates are also shown, Blue: Sn , Light grey: In, Grey : Pt, Red : O and White : H. The X and Y axis indicate the number of Hydroxyls and Oxygen added to the initial Pt-SA/ITO. The electrochemical conditions correspond to a potential U = 1.5 V vs SHE and pH = 1.

the nature of their active sites[46–51]. Li et al observed the formation of a stable Pt oxide during ORR on Pt single atoms (2.0 wt%) on graphitic carbon nitride (g-C_3N_4) derived N-doped carbon nanosheets (NCNS), which may suppress the adsorption and activation of O_2 and therefore be detrimental to ORR [52]. Cao et al. were able to achieve atomically dispersed $Fe_1(OH)_x$ on Pt nanoparticles (NPs), resulting in a 30-fold increase in mass activity compared to conventional catalysts and 100% CO selectivity over a wide temperature range for the preferential oxidation of CO in hydrogen. The in-situ XAS results revealed selective deposition of iron hydroxide on the surface of Pt NPs and illustrated that the $Fe_1(OH)_x$/Pt interface can easily react with CO and facilitate oxygen activation[53]. Furthermore, Cao and co-workers used operando XAS to study the formation of a high-valence HO-Co_1-N_2 (Single atomic Co supported on phosphorized carbon nitride) moiety and were able to successfully demonstrate the formation of the reaction intermediate H_2O-(HO-Co_1-N_2). Theoretical calculation results further confirmed that the highly oxidized and reconstructed Co1 single atoms decreased the energy barrier for water dissociation, thus resulting in high catalytic performance for HER in alkaline media[54].

To find the optimum coverage of -OH/-O/-OOH around the Pt-SA supported on ITO at varying electrochemical potential and for different Pt adsorption sites on the oxide, we used the Grand Canonical Basin Hopping [55–57] (GCBH) method (SI-S4). For this free energy surface (FES) exploration, we use the following mutations in our GCBH method:

A. The Pt-SA can move randomly over the ITO surface to find its most stable adsorption site.

B. The -OH/-O/-OOH coverage is mutated grand canonically to find the most stable coverage of the adsorbates on the Pt-SA. The changing adsorbate coverage under the electrochemical reaction condition can also modify the adsorption site. Hence, it's also important to simultaneously move the Pt-SA. The adsorbates can also attach to the ITO surface. Hence the adsorbates are not restricted to the Pt-SA but can access the whole catalyst surface.

C. The -OH/-H_2O groups already present on the ITO surface can move around and transfer onto the Pt-SA.

The three above-mentioned mutations are carried out simultaneously and one can affect the other so that the effect of all three needs to be studied simultaneously. The free energy surface explored

by GCBH relies on the formation free energy of PtO_xOH_y/ITO at pH = 1 and temperature(T) = 298K. This formation free energy is calculated as follows:

$$\text{Formation free Energy} = G\left(PtO_xOH_y(U)\right) - G(Pt\,SA_{ITO}(U)) - x\mu_O - y\mu_{OH}$$

Where, $G\left(PtO_xOH_y(U)\right)$ is the potential dependent energy of PtO_xOH_y and $G(Pt\,SA_{ITO}(U))$ is the potential depended energy fo the initial state of Pt-SA_{ITO} calculated via the surface charging method (SI-S3), μ_O is the chemical potential of oxygen and is obtained from the experimental formation energy of O with respect to water, since the O_2 molecule is not very well described within DFT. μ_{OH} is the chemical potential of hydroxyl. The chemical potential is evaluated via the following equations:

$$\mu_{OH} = \mu_{H_2O(l)} - (\mu_{H^+}(U,pH) + \mu_{e^-}(U,pH)); \mu_O = \mu_{H_2O(l)} - 2(\mu_{H^+}(U,pH) + \mu_{e^-}(U,pH));$$

Here, $\mu_{H_2O(l)}$ is the chemical potential of liquid water, at room temperature and 1 atm pressure take from the work of Munnik et al.[58] and $\mu_{H^+}(U,pH) + \mu_{e^-}(U,pH)$ can be calculated using the reference hydrogen electrode[59].

$$\mu_{H^+}(U,pH) + \mu_{e^-}(U,pH) = \frac{1}{2}\mu(H_2) - eU + k_B T pH \ln 10$$

One more important factor to keep in mind while exploring the free energy surface in these cases is the electrochemical potential at which we perform the GCBH. The catalytic active site would be different at varying electrochemical potential; hence in this work, we have chosen four different potentials to perform the GCBH, U = 0 V vs. SHE, U = 0.75 V vs. SHE, U = 1.4 V vs. SHE, and U = 1.5 V vs. SHE. We choose these potential values based on the experimental findings (Fig 1c) as already discussed. Our simulation model uses surface charging to maintain a constant potential, with surface charge adjusted to reach the desired potential. Fig 2 provides the free energy surface found via GCBH at U = 1.5 V vs. SHE and pH = 1, which corresponds to the experimental electrochemical potential for OER found for Pt-SA deposited on ITO.

We start with the most stable Pt-SA/ITO found in our previous work[45]. At any given catalytic active structure, there are three possibilities for evolution: (1) electrochemical addition of OH on the active site: $* + H_2O \rightarrow *OH + H^+ + e^-$, (2) After the addition of OH on the active site, this can

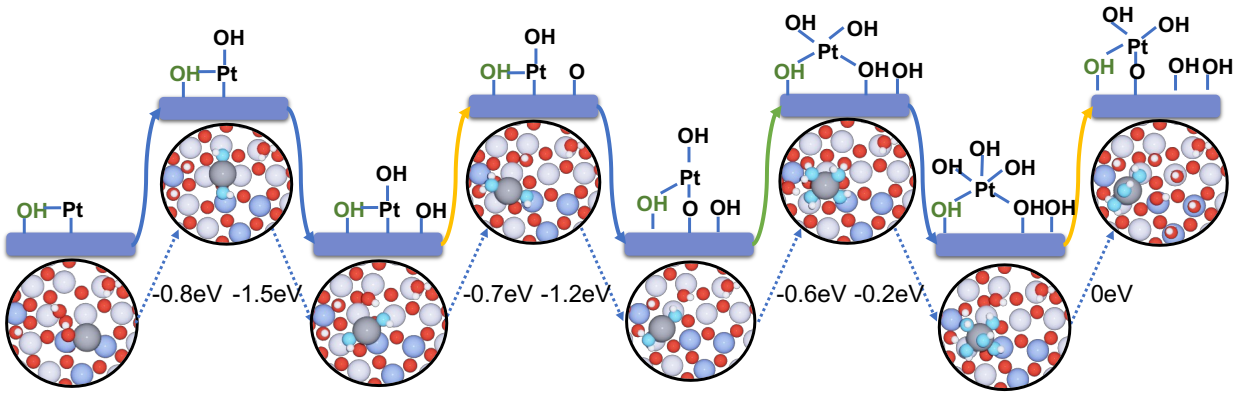

Figure 3: Full mechanism of formation of the active site for Pt-SA/ITO in electrochemical conditions found via GCBH. The blue arrow corresponds to the hydroxylation step, which is the first step of OER (* + H_2O → *OH + H^+ + e^-). The hydroxyl in green represents the hydroxyl already present on the surface in our initial Pt-SA structure. The yellow arrows correspond to the second OER step (* OH → *O + H^+ + e^-). The green arrow corresponds to water dissociation (H_2O → *OH + *H). The Final structure is the proposed active site for OER. The reaction free energies are given for each step and are calculated at a potential U = 1.5 V vs SHE and pH=1 for electrochemical steps. Blue: Sn , Light grey: In, Grey : Pt, Red : O and White : H. The hydroxyl and oxygens attached to Pt and directly participating in the active site are represented in light blue.

electrochemically convert to *O : *OH → *O + H^+ + e^- and (3) is the dissociative chemical adsorption of H_2O (H_2O → $H^+ + OH^-$) on the active site where the H^+ will adsorb on *O and OH^- will adsorb directly on the SA. We need to consider all the three possibilities above at each step to get to the active site of OER at the considered conditions. The reaction pathway to reach the active site at U = 1.5 V vs SHE is represented by differently colored arrows on the free energy surface. The blue arrow represents electrochemical reaction (1), yellow represents electrochemical reaction (2) and green represents chemical reaction (3). The numbers given inside the boxes in Figure 2 are the formation energy of PtO_xOH_y/ITO. To jump to the next configuration via reactions 1, 2 or 3 the thermodynamics should be favorable at a particular potential. The thermodynamically favored transformations are indicated by colored arrows in figure 2. This will then decide at any electrochemical potential what the configuration of the active site is.

Fig 3 provides the full pathway of forming the active site at U = 1.5 V vs SHE from Pt-SA/ITO (*) which were previously represented as arrows on Fig 2. We start with our initial structure for Pt-SA/ITO, where the Pt atom is already interacting with a hydroxyl present on the surface, which is represented in green throughout the reaction pathway. At the electrochemical potential of 1.5 V vs SHE, the first step is the adsorption of a hydroxyl via the reaction (1) (blue): * + H_2O → *OH + H^+ + e^-. The hydroxyl adsorbs on the Pt atom, causes a change in the adsorption site of the Pt atom and leads to the formation of a $Pt(OH)_2$ species. The Pt atom, which was previously

interacting with 2 Sn atoms, now interacts with 2 In atoms. In the next reaction step, Pt is once again hydroxylated, but one of the -OH from the previously formed $Pt(OH)_2$ group spills over on the ITO support so that a $Pt(OH)_2$ ITO-OH species is formed, with still 2 OH on the Pt (here ITO-OH represents the hydroxyl attached to ITO which spilled over on the surface). Concomitantly Pt moves to a Sn-In bridge site. The next more favorable step is to extract a proton via the reaction $*OH \rightarrow *O + H^+ + e^-$ from a neighboring hydroxyl present on the surface instead from the hydroxyl attached to $Pt(OH)_2$, leading to the formation of $Pt(OH)_2$ ITO-O. The surface oxygen species from ITO-O transfers onto the $Pt(OH)_2$ group in the following step, moving from the surface to a position immediately below the Pt, and another OH species occupies the vacant O site in the same concerted step to create $PtO(OH)_2$ITO-OH species. In the next step, we observe the dissociative adsorption of a H_2O molecule onto $PtO(OH)_2$ITO-OH, where H+ attaches to the O and OH attaches to Pt, to form $Pt(OH)_4$ITO-OH. This is followed by an electrochemical addition of OH to

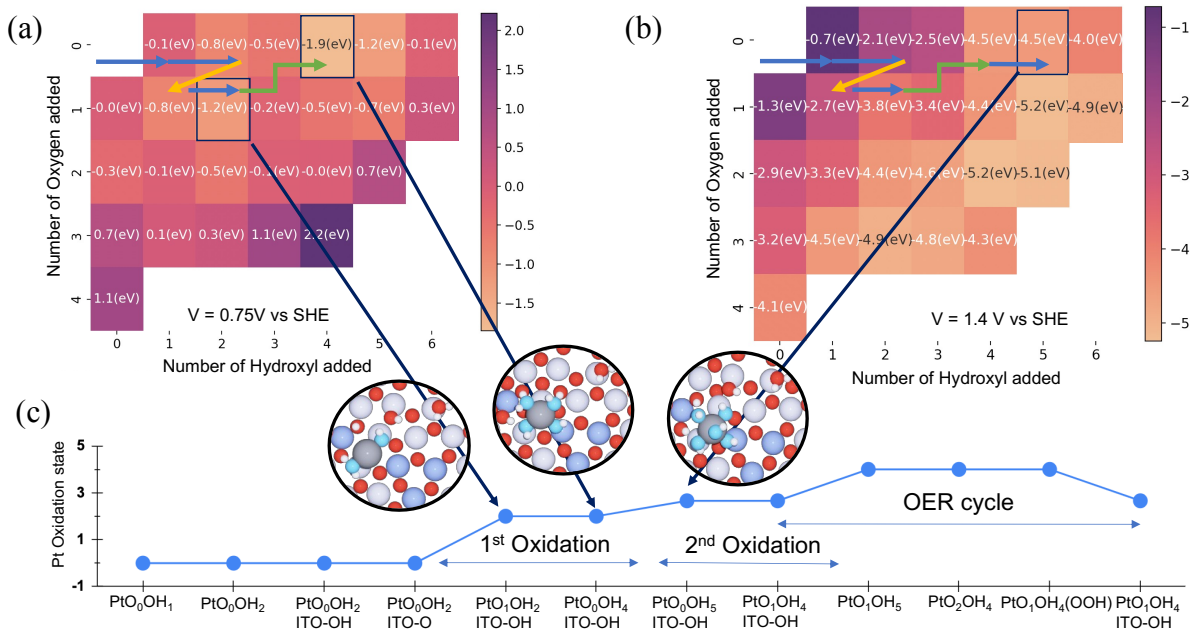

Figure 4: Free energy surface for Pt-SA/ITO in OER conditions at (a) U = 0.75V vs SHE (b) U = 1.4V vs SHE and pH=1. The black box on the free energy surface represents the energetically favorable composition for Pt-SA/ITO at the corresponding potential. The arrows represent the combination of reaction pathways needed to reach the favorable composition. (c) Oxidation state (OS) of the Pt atom as a function of the composition of the active site. The 1st oxidation of Pt from 0 →2 takes place at U = 0.75 V vs SHE, the second oxidation from 2→2.66 takes place at U = 1.4 V vs SHE and finally within the OER catalytic cycle, Pt cycles between the OS of 2.66 and 4.

the Pt site, making $Pt(OH)_5$ITO-OH, and finally in the next step of deprotonation of a *-OH from the Pt site, we form $PtO(OH)_4$ITO-OH which is the active site for OER.

Calculations also provide insights on the dependence of the Pt hydroxylation level on the electrochemical potential. We now depict the same free energy surface shown in Fig. 2 but with an electrochemical potential of 0.75 V and 1.4 V vs. SHE to show the potential-dependent formation process and the oxidation states (OS) of the active site. These electrochemical potentials are chosen to closely represent the oxidation peaks identified experimentally in the cyclic voltammogram. The free energy surface is shown in Fig. 4(a) at U = 0.75 V vs. SHE, and in (b), it is shown at U = 1.4 V vs. SHE. We find that the most stable active site composition is $PtO_0(OH)_4$ITO-OH at U = 0.75V versus SHE. The chemical route depicted by the arrows creates this active site. (PtO_0OH_1 → $PtO_0(OH)_2$ → $PtO_0(OH)_2$ITO-OH → $PtO_0(OH)_2$ITO-O → $PtO_1(OH)_2$ITO-OH → $PtO_0(OH)_4$ITO-OH). Along the reaction pathway, we also illustrate the Pt OS at various PtO_xOH_y compositions (Figure 4c). By comparing the Bader charge of Pt in the active site with the Bader charges of known Pt compounds with well-defined oxidation states, for example, OS 0 for Pt(111), OS 2 for PtO, OS 2.66 for Pt_2O_3, and OS 4 for PtO_2, the OS for each composition was estimated. PtO_0OH_1 has an OS of 0 in its initial state, which is similar to metallic Pt. Despite requiring four electrochemical steps to reach the state $Pt(OH)_2$ITO-O, the OS of Pt remains 0. This could be the result of ITO surface oxidation rather than Pt active site oxidation. When the composition changes to $PtO_1(OH)_2$ITO-OH in the following step, we see an increase in the OS to +2 because of the above-described migration of O to Pt accompanying the electrochemical addition of OH on ITO, which takes place at a potential of 0.75V versus SHE. The next composition of PtO_0OH_4 is formed by chemical dissociative adsorption of H_2O on PtO_1OH_2 which doesn't cause any change in the OS as this is a non-electrochemical step. At the electrochemical potential of 1.4 V vs SHE, the $PtO_0(OH)_4$ITO-OH can further oxidize to $PtO_0(OH)_5$ITO-OH, where the Pt OS is around 2.66. At a slightly higher potential of 1.5 V vs SHE, we observe the formation of the active site for the OER which is $PtO_1(OH)_4$ITO-OH. This step doesn't cause any change in the OS of the Pt, which means that this electrochemical step has caused further oxidation of ITO. At this potential, we also observe the extensive hydroxylation of

the support surface where the surface In and Sn sites gets completely covered with hydroxyls. This surface hydroxylation of ITO at positive potentials was also observed by Lebedev et al[31].

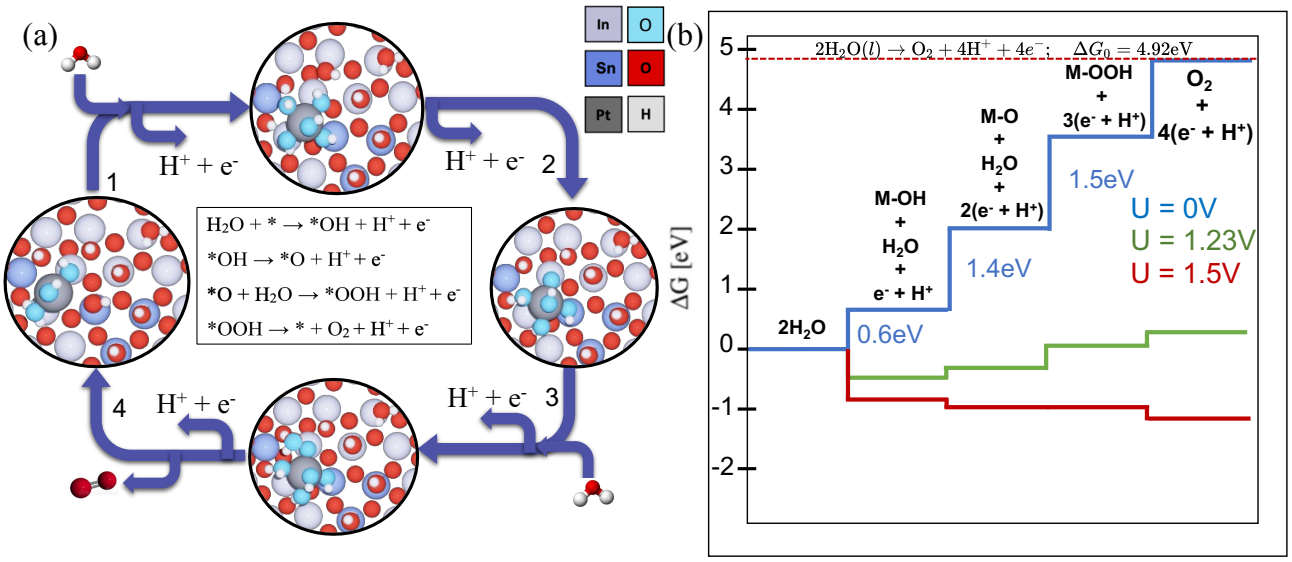

Figure 5: OER reaction mechanism on the active site of Pt-SA/ITO (PtO_1OH_4) found via GCBH as discussed in Fig 3, at the electrochemical reaction conditions (potential U = 1.5 V vs SHE). (a) 4 step OER reaction mechanism (b) Reaction energy profile at U = 0 V vs SHE(Blue), U = 1.23V vs SHE (Green) and U = 1.5 V vs SHE (Red).

In Fig 5, we finally investigate the reaction mechanism of OER starting from the "optimal" active site found via GCBH as discussed earlier, for a potential of 1.5V vs SHE. In the first reaction of the 4-step OER mechanism, the OH adsorbs on the active site at a bridge position between the Pt-SA and Sn. In the next step, a proton is evolved from another hydroxyl located on the bridging position of Pt and In. Deprotonation of other hydroxyl groups are not as favorable; this means that the acidity of the various hydroxyls is very different. After the deprotonation another hydroxyl adorbs on the *O forming *OOH. This then produces O_2 and regenerates the active site. The reaction diagram of this OER pathway is given in Fig 5(b), where we find the third step to be the rate determining step with an overpotential of 0.27 V vs SHE. This overpotential value is in excellent agreement with the experimental data (0.27 V). It should be noted however that exact coincidence is fortuitous, since calculations present several approximations in model and method aspects. During this catalytic cycle the oxidation state of Pt cycles between 2.66 and 4. Not all the 4 electrons required for the oxygen evolution reaction come from Pt-SA, other electrons come from the reduction of the ITO surface itself. It becomes abundantly evident that there is a

significant discrepancy of 0.3V vs. SHE between the overpotential computed using the active site formed in electrooxidation conditions and the overpotential calculated using the initial non-optimal active site. Only the approach using the active site determined at U=1.5 V vs SHE is self-consistent and physically meaningful, since the onset potential is 1.5 V, potential for which the determined active site is stable. This emphasizes how crucial it is to identify, using operando computational approaches, the composition and geometry active site under the reaction conditions which may change greatly due to the numerous adsorbates from the original initial structure. This change could be in both the adsorption site of the Pt atom on the support and in the composition of the active site in terms of ligands. This computational approach also helped us identify the active site composition at oxidation peaks to understand the electrocatalytic process and species involved, as well as determining the oxidation state of Pt-SA at these peaks. Such a first-principle determination of the nature of the active site in electrocatalytic conditions, coupled with experimental operando characterization, opens major perspectives for our fundamental understanding of electrocatalysis and for the design of efficient catalysts.

ACKNOWLEDGEMENTS

This work was supported by the grant DE-SC0020125 from the US Department of Energy, Office of Science, Basic Energy Science Program. This research used resources of the Innovative and Novel Computational Impact on Theory and Experiment (INCITE) program at the Argonne Leadership Computing Facility (theta machine, grant name 'DynCatalysis'), a U.S. Department of Energy Office of Science User Facility operated under Contract DE-AC02-06CH11357. This work used computational and storage services associated with the Hoffman2 Shared Cluster provided by the UCLA Institute for Digital Research and Education Research Technology Group. This research used the resources of the National Energy Research Scientific Computing Center (NERSC), a U.S. Department of Energy Office of Science User Facility operated under Contract No. DE-AC02-05CH11231. The authors want to thank XSEDE SDSC's Comet, Expanse Supercomputer, and Bridges PSC for the computation time.

SUPPORTING INFORMATION AVAILABLE:

- Computational Methods: Full details on the computational methods used in the work, details on surface charging method to calculate the potential defendant free energy of the species, full details on the Grand Canonical Basin Hopping method and the details of the Pt-SA/ITO initial structure derived from our previous work.

REFERENCES

(1) Fabbri, E.; Habereder, A.; Waltar, K.; Kötz, R.; Schmidt, T. J. Developments and Perspectives of Oxide-Based Catalysts for the Oxygen Evolution Reaction. *Catal. Sci. Technol.* **2014**, *4* (11), 3800–3821. https://doi.org/10.1039/c4cy00669k.

(2) Zhang, X.; Bieberle-Hütter, A. Modeling and Simulations in Photoelectrochemical Water Oxidation: From Single Level to Multiscale Modeling. *ChemSusChem* **2016**, *9* (11), 1223–1242. https://doi.org/10.1002/cssc.201600214.

(3) Nørskov, J. K.; Rossmeisl, J.; Logadottir, A.; Lindqvist, L.; Kitchin, J. R.; Bligaard, T.; Jónsson, H. Origin of the Overpotential for Oxygen Reduction at a Fuel-Cell Cathode. *J. Phys. Chem. B* **2004**, *108* (46), 17886–17892. https://doi.org/10.1021/jp047349j.

(4) Rossmeisl, J.; Qu, Z. W.; Zhu, H.; Kroes, G. J.; Nørskov, J. K. Electrolysis of Water on Oxide Surfaces. *J. Electroanal. Chem.* **2007**, *607* (1–2), 83–89. https://doi.org/10.1016/j.jelechem.2006.11.008.

(5) Qiao, B.; Wang, A.; Yang, X.; Allard, L. F.; Jiang, Z.; Cui, Y.; Liu, J.; Li, J.; Zhang, T. Single-Atom Catalysis of CO Oxidation Using Pt1/FeOx. *Nat Chem* **2011**, *3* (8), 634–641. https://doi.org/10.1038/nchem.1095.

(6) Peterson, E. J.; DeLaRiva, A. T.; Lin, S.; Johnson, R. S.; Guo, H.; Miller, J. T.; Kwak, J. H.; Peden, C. H. F.; Kiefer, B.; Allard, L. F.; Ribeiro, F. H.; Datye, A. K. Low-Temperature Carbon Monoxide Oxidation Catalysed by Regenerable Atomically Dispersed Palladium on Alumina. *Nat Commun* **2014**, *5* (1), 4885. https://doi.org/10.1038/ncomms5885.

(7) DeRita, L.; Resasco, J.; Dai, S.; Boubnov, A.; Thang, H. V.; Hoffman, A. S.; Ro, I.; Graham, G. W.; Bare, S. R.; Pacchioni, G.; Pan, X.; Christopher, P. Structural Evolution of Atomically Dispersed Pt Catalysts Dictates Reactivity. *Nat Mater* **2019**, *18* (7), 746–751. https://doi.org/10.1038/s41563-019-0349-9.

(8) Yoo, M.; Yu, Y. S.; Ha, H.; Lee, S.; Choi, J. S.; Oh, S.; Kang, E.; Choi, H.; An, H.; Lee, K. S.; Park, J. Y.; Celestre, R.; Marcus, M. A.; Nowrouzi, K.; Taube, D.; Shapiro, D. A.; Jung, W. C.; Kim, C.; Kim, H. Y. A Tailored Oxide Interface Creates Dense Pt Single-Atom Catalysts with High Catalytic Activity. *Energy Environ Sci* **2020**, *13* (4), 1231-1239. https://doi.org/10.1039/c9ee03492g.

(9) Yan, H.; Lin, Y.; Wu, H.; Zhang, W.; Sun, Z.; Cheng, H.; Liu, W.; Wang, C.; Li, J.; Huang, X.; Yao, T.; Yang, J.; Wei, S.; Lu, J. Bottom-up Precise Synthesis of Stable Platinum Dimers on Graphene. *Nat Commun* **2017**, *8* (1), 1070. https://doi.org/10.1038/S41467-017-01259-Z.

(10) Li, J.; Guan, Q.; Wu, H.; Liu, W.; Lin, Y.; Sun, Z.; Ye, X.; Zheng, X.; Pan, H.; Zhu, J.; Chen, S.; Zhang, W.; Wei, S.; Lu, J. Highly Active and Stable Metal Single-Atom Catalysts Achieved by Strong Electronic Metal-Support Interactions. *J Am Chem Soc* **2019**, *141* (37), 14515–14519. https://doi.org/10.1021/JACS.9B06482.

(11) Cheng, N.; Stambula, S.; Wang, D.; Banis, M. N.; Liu, J.; Riese, A.; Xiao, B.; Li, R.; Sham, T. K.; Liu, L. M.; Botton, G. A.; Sun, X. Platinum Single-Atom and Cluster Catalysis of the Hydrogen Evolution Reaction. *Nature Communications* **2016**, *7* (1), 1–9. https://doi.org/10.1038/ncomms13638.

(12) Chen, Y.; Ji, S.; Chen, C.; Peng, Q.; Wang, D.; Li, Y. Single-Atom Catalysts: Synthetic Strategies and Electrochemical Applications. *Joule* **2018**, *2* (7), 1242–1264. https://doi.org/10.1016/j.joule.2018.06.019.

(13) Shang, R.; Steinmann, S. N.; Xu, B. Q.; Sautet, P. Mononuclear Fe in N-Doped Carbon: Computational Elucidation of Active Sites for Electrochemical Oxygen Reduction and Oxygen Evolution Reactions. *Catal Sci Technol* **2020**, *10* (4), 1006–1014. https://doi.org/10.1039/C9CY01935A.

(14) Kumari, S.; Masubuchi, T.; White, H. S.; Alexandrova, A.; Anderson, S. L.; Sautet, P. Electrocatalytic Hydrogen Evolution at Full Atomic Utilization over ITO-Supported Sub-Nano Ptn Clusters: High, Size-Dependent Activity Controlled by Fluxional Pt Hydride Species. **2022**. https://doi.org/10.26434/CHEMRXIV-2022-5870P.

(15) Lee, B. H.; Park, S.; Kim, M.; Sinha, A. K.; Lee, S. C.; Jung, E.; Chang, W. J.; Lee, K. S.; Kim, J. H.; Cho, S. P.; Kim, H.; Nam, K. T.; Hyeon, T. Reversible and Cooperative Photoactivation of Single-Atom Cu/TiO2 Photocatalysts. *Nat Mater* **2019**, *18* (6), 620–626. https://doi.org/10.1038/s41563-019-0344-1.

(16) Daelman, N.; Capdevila-Cortada, M.; López, N. Dynamic Charge and Oxidation State of Pt/CeO2 Single-Atom Catalysts. *Nat Mater* **2019**, *18* (11), 1215–1221. https://doi.org/10.1038/s41563-019-0444-y.

(17) Liu, P.; Zhao, Y.; Qin, R.; Mo, S.; Chen, G.; Gu, L.; Chevrier, D. M.; Zhang, P.; Guo, Q.; Zang, D.; Wu, B.; Fu, G.; Zheng, N. Catalysis: Photochemical Route for Synthesizing Atomically Dispersed Palladium Catalysts. *Science* **2016**, *352* (6287), 797-800. https://doi.org/10.1126/science.aaf5251.

(18) Gu, J.; Hsu, C. S.; Bai, L.; Chen, H. M.; Hu, X. Atomically Dispersed Fe3+ Sites Catalyze Efficient CO2 Electroreduction to CO. *Science* **2019**, *364* (6445), 1091–1094. https://doi.org/10.1126/SCIENCE.AAW7515

(19) Xiao, M.; Zhu, J.; Li, G.; Li, N.; Li, S.; Cano, Z. P.; Ma, L.; Cui, P.; Xu, P.; Jiang, G.; Jin, H.; Wang, S.; Wu, T.; Lu, J.; Yu, A.; Su, D.; Chen, Z. A Single-Atom Iridium Heterogeneous Catalyst in Oxygen Reduction Reaction. *Angewandte Chemie - International Edition* **2019**, *58* (28), 9640-9645. https://doi.org/10.1002/anie.201905241.

(20) Tang, Y.; Asokan, C.; Xu, M.; Graham, G. W.; Pan, X.; Christopher, P.; Li, J.; Sautet, P. Rh Single Atoms on TiO2 Dynamically Respond to Reaction Conditions by Adapting Their Site. *Nat Commun* **2019**, *10* (1), 4488. https://doi.org/10.1038/s41467-019-12461-6.

(21) Yang, X. F.; Wang, A.; Qiao, B.; Li, J.; Liu, J.; Zhang, T. Single-Atom Catalysts: A New Frontier in Heterogeneous Catalysis. *Acc Chem Res* **2013**, *46* (8), 1740–1748. https://doi.org/10.1021/AR300361M.

(22) Zhang, B.; Sun, G.; Ding, S.; Asakura, H.; Zhang, J.; Sautet, P.; Yan, N. Atomically Dispersed Pt_1 –Polyoxometalate Catalysts: How Does Metal–Support Interaction Affect Stability and Hydrogenation Activity? *J Am Chem Soc* **2019**, *141*(20), 8185-8197. https://doi.org/10.1021/jacs.9b00486.

(23) Zhang, L.; Doyle-Davis, K.; Sun, X. Pt-Based Electrocatalysts with High Atom Utilization Efficiency: From Nanostructures to Single Atoms. *Energy Environ Sci* **2019**, *12* (2), 492–517. https://doi.org/10.1039/C8EE02939C.

(24) García-Mota, M.; Vojvodic, A.; Metiu, H.; Man, I. C.; Su, H. Y.; Rossmeisl, J.; Nørskov, J. K. Tailoring the Activity for Oxygen Evolution Electrocatalysis on Rutile TiO2(110) by Transition-Metal Substitution. *ChemCatChem* **2011**, *3* (10), 1607-1611. https://doi.org/10.1002/cctc.201100160.
(25) Zhao, Y.; Yang, K. R.; Wang, Z.; Yan, X.; Cao, S.; Ye, Y.; Dong, Q.; Zhang, X.; Thorne, J. E.; Jin, L.; Materna, K. L.; Trimpalis, A.; Bai, H.; Fakra, S. C.; Zhong, X.; Wang, P.; Pan, X.; Guo, J.; Flytzani-Stephanopoulos, M.; Brudvig, G. W.; Batista, V. S.; Wang, D. Stable Iridium Dinuclear Heterogeneous Catalysts Supported on Metal-Oxide Substrate for Solar Water Oxidation. *Proc Natl Acad Sci U S A* **2018**, *115* (12), 2902-2907. https://doi.org/10.1073/pnas.1722137115.
(26) Zhao, Y.; Yan, X.; Yang, K. R.; Cao, S.; Dong, Q.; Thorne, J. E.; Materna, K. L.; Zhu, S.; Pan, X.; Flytzani-Stephanopoulos, M.; Brudvig, G. W.; Batista, V. S.; Wang, D. End-On Bound Iridium Dinuclear Heterogeneous Catalysts on WO3 for Solar Water Oxidation. *ACS Cent Sci* **2018**, *4* (9), 1166–1172. https://doi.org/10.1021/acscentsci.8b00335.
(27) Zhu, C.; Shi, Q.; Feng, S.; Du, D.; Lin, Y. Single-Atom Catalysts for Electrochemical Water Splitting. *ACS Energy Lett* **2018**, *3* (7), 1713–1721. https://doi.org/10.1021/ACSENERGYLETT.8B00640.
(28) Fei, H.; Dong, J.; Feng, Y.; Allen, C. S.; Wan, C.; Volosskiy, B.; Li, M.; Zhao, Z.; Wang, Y.; Sun, H.; An, P.; Chen, W.; Guo, Z.; Lee, C.; Chen, D.; Shakir, I.; Liu, M.; Hu, T.; Li, Y.; Kirkland, A. I.; Duan, X.; Huang, Y. General Synthesis and Definitive Structural Identification of MN4C4 Single-Atom Catalysts with Tunable Electrocatalytic Activities. *Nat Catal* **2018**, *1* (1), 63–72. https://doi.org/10.1038/s41929-017-0008-y.
(29) Cao, L.; Luo, Q.; Chen, J.; Wang, L.; Lin, Y.; Wang, H.; Liu, X.; Shen, X.; Zhang, W.; Liu, W.; Qi, Z.; Jiang, Z.; Yang, J.; Yao, T. Dynamic Oxygen Adsorption on Single-Atomic Ruthenium Catalyst with High Performance for Acidic Oxygen Evolution Reaction. *Nat Commun* **2019**, *10* (1), 4849. https://doi.org/10.1038/s41467-019-12886-z.
(30) Ganguli, S.; Das, S.; Kumari, S.; Inta, H. R.; Tiwari, A. K.; Mahalingam, V. Effect of Intrinsic Properties of Anions on the Electrocatalytic Activity of NiCo2O4 and NiCo2OxS4- x Grown by Chemical Bath Deposition. *ACS Omega* **2018**, *3* (8), 9066–9074. https://doi.org/10.1021/ACSOMEGA.8B00952
(31) Lebedev, D.; Ezhov, R.; Heras-Domingo, J.; Comas-Vives, A.; Kaeffer, N.; Willinger, M.; Solans-Monfort, X.; Huang, X.; Pushkar, Y.; Copéret, C. Atomically Dispersed Iridium on Indium Tin Oxide Efficiently Catalyzes Water Oxidation. *ACS Cent Sci* **2020**, *6* (7), 1189–1198. https://doi.org/10.1021/ACSCENTSCI.0C00604
(32) Babic, U.; Suermann, M.; Büchi, F. N.; Gubler, L.; Schmidt, T. J. Critical Review—Identifying Critical Gaps for Polymer Electrolyte Water Electrolysis Development. *J Electrochem Soc* **2017**, *164* (4), F387. https://doi.org/10.1149/2.1441704jes.
(33) Suen, N. T.; Hung, S. F.; Quan, Q.; Zhang, N.; Xu, Y. J.; Chen, H. M. Electrocatalysis for the Oxygen Evolution Reaction: Recent Development and Future Perspectives. *Chemical Society Reviews*, **2017**, *46*(2), 337-365. https://doi.org/10.1039/c6cs00328a.
(34) Hosseini Benhangi, P.; Gyenge, E.; Alfantazi, A.; Liang, Q.; Brocks, G.; Bieberle-Hütter, A. Oxygen Evolution Reaction (OER) Mechanism under Alkaline and Acidic Conditions. *Journal of Physics: Energy* **2021**, *3* (2), 026001. https://doi.org/10.1088/2515-7655/ABDC85.
(35) Eranna, G.; Joshi, B. C.; Runthala, D. P.; Gupta, R. P. Oxide Materials for Development of Integrated Gas Sensors - A Comprehensive Review. *Critical Reviews in Solid State and*

Materials Sciences **2004**, *29* (3–4), 111–188. https://doi.org/10.1080/10408430490888977.
(36) Ye, J.; Liu, C.; Mei, D.; Ge, Q. Active Oxygen Vacancy Site for Methanol Synthesis from CO2 Hydrogenation on In2O3(110): A DFT Study. *ACS Catal* **2013**, *3* (6), 1296–1306. https://doi.org/10.1021/cs400132a.
(37) Ye, J.; Liu, C.; Ge, Q. DFT Study of CO 2 Adsorption and Hydrogenation on the in 2O 3 Surface. *Journal of Physical Chemistry C* **2012**, *116* (14), 7817–7825. https://doi.org/10.1021/JP3004773
(38) Hartnagel, H.; A. L. Dawar; C. Jagadish; A. K. Jain. *Semiconducting Transparent Thin Films*; CRC Press, **1995**.
(39) von Weber, A.; Anderson, S. L. Electrocatalysis by Mass-Selected Ptn Clusters. *Acc Chem Res* **2016**, *49* (11), 2632–2639. https://doi.org/10.1021/acs.accounts.6b00387.
(40) von Weber, A.; Baxter, E. T.; White, H. S.; Anderson, S. L. Cluster Size Controls Branching between Water and Hydrogen Peroxide Production in Electrochemical Oxygen Reduction at Ptn/ITO. *Journal of Physical Chemistry C* **2015**, *119* (20), 11160–11170. https://doi.org/10.1021/jp5119234.
(41) von Weber, A.; Baxter, E. T.; White, H. S.; Anderson, S. L. Cluster Size Controls Branching between Water and Hydrogen Peroxide Production in Electrochemical Oxygen Reduction at Ptn/ITO. *Journal of Physical Chemistry C* **2015,** *119*(20), 11160-11170. https://doi.org/10.1021/jp5119234.
(42) von Weber, A.; Baxter, E. T.; Proch, S.; Kane, M. D.; Rosenfelder, M.; White, H. S.; Anderson, S. L. Size-Dependent Electronic Structure Controls Activity for Ethanol Electro-Oxidation at Pt n /Indium Tin Oxide (n = 1 to 14). *Physical Chemistry Chemical Physics* **2015**, *17* (27), 17601–17610. https://doi.org/10.1039/C5CP01824B.
(43) Mizuhashi, M. Electrical Properties of Vacuum-Deposited Indium Oxide and Indium Tin Oxide Films. *Thin Solid Films* **1980**, *70* (1), 91–100. https://doi.org/10.1016/0040-6090(80)90415-0.
(44) Kumari, S.; Sautet, P. Highly Dispersed Pt Atoms and Clusters on Hydroxylated Indium Tin Oxide: A View from First-Principles Calculations. *J Mater Chem A Mater* **2021**, *9* (28), 15724–15733. https://doi.org/10.1039/d1ta03177e.
(45) Dou, J.; Sun, Z.; Opalade, A. A.; Wang, N.; Fu, W.; Tao, F. Operando Chemistry of Catalyst Surfaces during Catalysis. *Chem Soc Rev* **2017**, *46* (7), 2001–2027. https://doi.org/10.1039/C6CS00931J.
(46) Friebel, D.; Miller, D. J.; O'Grady, C. P.; Anniyev, T.; Bargar, J.; Bergmann, U.; Ogasawara, H.; Wikfeldt, K. T.; Pettersson, L. G. M.; Nilsson, A. In Situ X-Ray Probing Reveals Fingerprints of Surface Platinum Oxide. *Physical Chemistry Chemical Physics* **2010**, *13* (1), 262–266. https://doi.org/10.1039/C0CP01434F.
(47) Banis, M. N.; Yadegari, H.; Sun, Q.; Regier, T.; Boyko, T.; Zhou, J.; Yiu, Y. M.; Li, R.; Hu, Y.; Sham, T. K.; Sun, X. Revealing the Charge/Discharge Mechanism of Na–O2 Cells by in Situ Soft X-Ray Absorption Spectroscopy. *Energy Environ Sci* **2018**, *11* (8), 2073–2077. https://doi.org/10.1039/C8EE00721G.
(48) Zhang, J.; Zhao, Y.; Guo, X.; Chen, C.; Dong, C. L.; Liu, R. S.; Han, C. P.; Li, Y.; Gogotsi, Y.; Wang, G. Single Platinum Atoms Immobilized on an MXene as an Efficient Catalyst for the Hydrogen Evolution Reaction. *Nature Catalysis 2018 1:12* **2018**, *1* (12), 985–992. https://doi.org/10.1038/s41929-018-0195-1.

(49) Lu, Y.; Wang, J.; Yu, L.; Kovarik, L.; Zhang, X.; Hoffman, A. S.; Gallo, A.; Bare, S. R.; Sokaras, D.; Kroll, T.; Dagle, V.; Xin, H.; Karim, A. M. Identification of the Active Complex for CO Oxidation over Single-Atom Ir-on-MgAl2O4 Catalysts. *Nature Catalysis 2018 2:2* **2018**, *2* (2), 149–156. https://doi.org/10.1038/s41929-018-0192-4.

(50) Dessal, C.; Len, T.; Morfin, F.; Rousset, J. L.; Aouine, M.; Afanasiev, P.; Piccolo, L. Dynamics of Single Pt Atoms on Alumina during CO Oxidation Monitored by Operando X-Ray and Infrared Spectroscopies. *ACS Catal* **2019**, *9* (6), 5752–5759. https://doi.org/10.1021/ACSCATAL.9B00903

(51) Li, J.; Banis, M. N.; Ren, Z.; Adair, K. R.; Doyle-Davis, K.; Meira, D. M.; Finfrock, Y. Z.; Zhang, L.; Kong, F.; Sham, T. K.; Li, R.; Luo, J.; Sun, X. Unveiling the Nature of Pt Single-Atom Catalyst during Electrocatalytic Hydrogen Evolution and Oxygen Reduction Reactions. *Small* **2021**, *17* (11), 2007245. https://doi.org/10.1002/SMLL.202007245.

(52) Cao, L.; Liu, W.; Luo, Q.; Yin, R.; Wang, B.; Weissenrieder, J.; Soldemo, M.; Yan, H.; Lin, Y.; Sun, Z.; Ma, C.; Zhang, W.; Chen, S.; Wang, H.; Guan, Q.; Yao, T.; Wei, S.; Yang, J.; Lu, J. Atomically Dispersed Iron Hydroxide Anchored on Pt for Preferential Oxidation of CO in H2. *Nature 2019 565:7741* **2019**, *565* (7741), 631–635. https://doi.org/10.1038/s41586-018-0869-5.

(53) Cao, L.; Luo, Q.; Liu, W.; Lin, Y.; Liu, X.; Cao, Y.; Zhang, W.; Wu, Y.; Yang, J.; Yao, T.; Wei, S. Identification of Single-Atom Active Sites in Carbon-Based Cobalt Catalysts during Electrocatalytic Hydrogen Evolution. *Nature Catalysis 2018 2:2* **2018**, *2* (2), 134–141. https://doi.org/10.1038/s41929-018-0203-5.

(54) Sun, G.; Sautet, P. Metastable Structures in Cluster Catalysis from First-Principles: Structural Ensemble in Reaction Conditions and Metastability Triggered Reactivity. *J Am Chem Soc* **2018**, *140* (8), 2812–2820. https://doi.org/10.1021/JACS.7B11239

(55) Sun, G.; Alexandrova, A. N.; Sautet, P. Structural Rearrangements of Subnanometer Cu Oxide Clusters Govern Catalytic Oxidation. *ACS Catal* **2020**, *10* (9), 5309–5317. https://doi.org/10.1021/ACSCATAL.0C00824

(56) Sun, G.; Alexandrova, A. N.; Sautet, P. Pt8 Cluster on Alumina under a Pressure of Hydrogen: Support-Dependent Reconstruction from First-Principles Global Optimization. *J Chem Phys* **2019**, *151* (19), 194703. https://doi.org/10.1063/1.5129296.

(57) Munnik, P.; de Jongh, P. E.; de Jong, K. P. Recent Developments in the Synthesis of Supported Catalysts. *Chemical Reviews*. American Chemical Society July 22, 2015, pp 6687–6718. https://doi.org/10.1021/cr500486u.

(58) Peterson, A. A.; Abild-Pedersen, F.; Studt, F.; Rossmeisl, J.; Nørskov, J. K. How Copper Catalyzes the Electroreduction of Carbon Dioxide into Hydrocarbon Fuels. *Energy Environ Sci* **2010**, *3* (9), 1311–1315. https://doi.org/10.1039/C0EE00071J.